PAPER

www.rsc.org/loc

Electrophoretic manipulation of single DNA molecules in nanofabricated capillaries†

L. C. Campbell,[a] M. J. Wilkinson,[b] A. Manz,[c] P. Camilleri[b] and C. J. Humphreys*[a]

[a] *University of Cambridge, Department of Materials Science and Metallurgy, Pembroke Street, Cambridge, UK CB2 3Q2. E-mail: colin.humphreys@msm.cam.ac.uk*

[b] *GSK Medicines Research Centre, Gunnels Wood Road, Stevenage, Herts, UK SG1 2NY*

[c] *Department of Chemistry, Imperial College, South Kensington, London, UK SW7 2AY*

Received 8th October 2003, Accepted 9th February 2004
First published as an Advance Article on the web 12th March 2004

We demonstrate the use of nanofabricated capillaries, integrated as part of a microfluidic structure, to study the electrophoretic behaviour of single, fluorescently-labelled, molecules of DNA as a function of capillary size. The nanocapillaries, fabricated using a focused ion beam, have cross-sections down to 150 × 180 nm. Control of single-molecule direction and velocity was achieved using voltage manipulation. DNA mobility was found to increase with decreasing cross-section, which we interpret in terms of reduced electro-osmotic counter-flow. Such nanofabricated capillaries as part of larger fluidic structures have great potential for biotechnology, particularly single molecule manipulation and analysis.

Introduction

Microfabricated devices have been constructed previously to explore DNA movement in an electric field. These have incorporated channels, planar slits and chambers, primarily to achieve movement and separation of heterogeneous DNA populations.[1–5] To investigate the behaviour of single DNA molecules constrained in sub-micron channels, we have constructed nanocapillaries. By nanocapillary we mean a channel having sub-micron dimensions in cross-section and covered to form a tube.

Over the last decade there has been great success in the development of microfluidic devices for biochemical analysis. In the area of DNA electrophoresis and analysis microfabricated structures with characteristic dimensions of microns to tens of microns have included channels, planar slits (sub-micron height but many microns in width) and chambers, primarily to achieve movement and separation of heterogeneous populations.[1–5] A natural progression is to extend miniaturization to devices with characteristic dimensions in the nanometre range, with an emphasis on single molecule analysis rather than the separation of populations. Nanofabricated capillaries, combined with other microfabricated devices, offer opportunities for extending single-molecule analysis. The existence of such structures has already been cited as a prerequisite for molecular mapping using near field optics.[5] Nanofluidics could also allow DNA sequencing by ionic conductance, as assessed recently using natural nanopores inserted into lipid bilayers and exposed to an electric field,[6,7] to be carried out 'on chip'.

Experimental

Fabrication of nanocapillaries

This fabrication involves a number of steps beginning with the formation of nanochannels in silicon which are then covered to produce nanocapillaries.

Milling of nanochannels

The silicon was (100) oriented, p-type (boron doped) and supplied as 3 inch diameter wafers, 400 μm thick, with a single polished face (Goodfellow, Cambridge). Squares of the desired size, sides ~1.5–2 cm, were cleaved from the wafer and 3.5 mm diameter holes for injection wells were cut using an ultrasonic disk cutter (Gatan). The back face of the silicon was polished to ensure a watertight seal to the intermediate PDMS layer. Finally the silicon was mounted on a stub using carbon tape and inserted into the focused ion beam (FIB) instrument, a fully computer controlled FEI 200 series workstation with a 30 kV Ga^+ beam extracted from a liquid metal ion source. When operating at the minimum beam current of 1 pA, the full-width half-maximum beam diameter is ~8 nm.[8] The system is fully computer controlled and features iodine enhanced etch and platinum deposition capabilities. The milled nanochannel layout is shown in Fig. 1a. The three smallest nanochannels were milled at a beam current of 4 pA, the larger channels were milled at 350 pA. All channels were milled using the workstation's enhanced etch facility: iodine gas was introduced near the sample surface during milling to enhance the sputter yield and minimize redeposition of removed material.[9,10]

Fabrication of glass master cover-slip structure

This structure with nine cover-slip patterns in a 3 × 3 array was patterned by UV lithography. A standard soda-lime glass microscope slide, measuring 7.5 × 5 cm was used as the substrate for patterning. The standard procedure for UV lithography was followed: the substrate was cleaned and coated with a positive photo-resist (*i.e.* exposed photo-resist defines the area to be etched). Then the desired pattern was exposed using a UV stepping laser system, developed, and etched to leave negatives of the final cover-slip structure. Exposure and development was carried out using conventional methodology employing a photo-resist coated on glass and a direct laser system (Heidelberg Instruments Mikrotechnik GmbH, 69126 Heidelberg, Germany). Exposed glass was etched using a 7:1 NH_4F:HF buffered etch solution for 11 min to give an estimated etch depth of 10 μm. After the desired etch time the substrate was immersed in water to halt the etch process and air-dried. The remaining (unexposed) photo-resist was stripped from the glass using DMF, leaving negatives of the desired cover-slip structure. The glass was cleaned by soaking in a 10:1:1 water:isopropyl alcohol (IPA):HCl solution overnight. This was followed by soaking for 3 min in each of dimethylformamide (DMF), chloroform, IPA and acetone in an ultrasonic bath, rinsing in water after each step. The substrate was dried first in air and then in an oven at 220 °C for 30 min.

† Electronic supplementary information (ESI) available: Four videoclips showing the movement of DNA molecules in nanocapillaries. See http://www.rsc.org/suppdata/lc/b3/b312592k/

DOI: 10.1039/b312592k

Casting of polydimethylsiloxane (PDMS)

The glass master structure was cleaned, and PDMS base and curing agent (Sylgard® 184, Dow Corning) were mixed in a ratio of 10:1 by volume and degassed in a vacuum. The PDMS was then poured over the desired mold and cured (2 h at 60 °C). Once cured, the PDMS was carefully peeled away from the mold.

Assembly and filling of nanocapillary structure

With the aid of a binocular microscope alignment of the FIB channels and the PDMS coverslip was achieved visually, ensuring that air bubbles between the two surfaces were absent. Filling this capillary structure was not trivial: initially it was necessary to fill with isopropyl alcohol, followed by a non-ionic surfactant (0.01% v/v Triton X-100), and finally the running buffer solution (10 mM Tris-HCl, pH 7.4, 8 mM ionic strength). Liquids were introduced using a 1 ml syringe either by capillary action, or by applying gentle suction to an empty injection well at the other end of the channel. The reservoir channel leading from that well would then be filled. The second reservoir channel was then filled in the same way. Finally a solution of double stranded λ-DNA was introduced, previously stained with the intercalating florescent dye YOYO-1 (Molecular Probes). The results presented here were obtained using a 20 pM (0.6 μg ml^{-1}) solution of λ-DNA (48.5 kbp, Sigma Chemical Co.) in the same running buffer solution of 10 mM Tris-HCl, pH 7.4, labelled with YOYO-1 at a base pair:dye ratio of 10:1.

Electrodes and voltage control

Electrodes were made from insulated copper wire (0.315 mm diameter) with the ends stripped and inserted into the sample wells. Power was supplied by a standard 9 V battery. The voltage applied across the fluidic device was monitored during experiments using a digital multimeter. A simple variable resistor circuit was used to provide variable voltage. Experiments were carried out at ambient temperature (21 ± 1 °C).

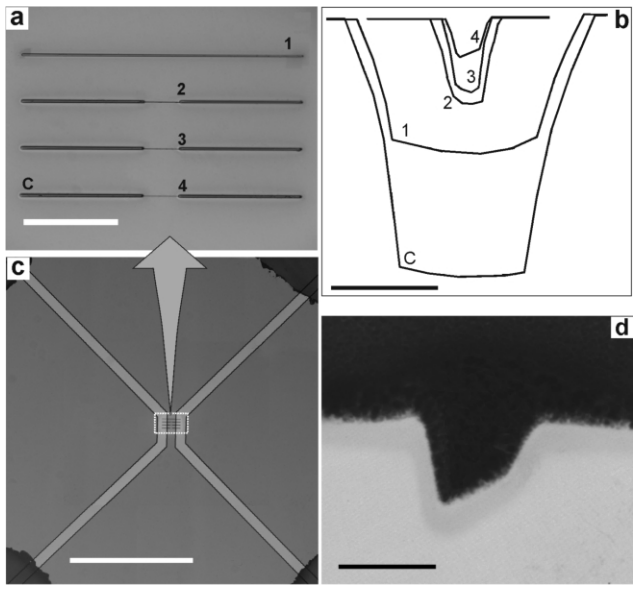

Fig. 1 Focused ion beam milled channels. (a) The silicon surface showing channel layout. Channel 1 is 150 μm long, channels 2–4, were 20 μm long with larger connecting channels (C, 1 × 1.2 μm cross-section) to either side. Channels 1 and C were milled with beam current of 350 pA, all others were milled at 4 pA. Scale bar = 50 μm. (b) Topographic cross-sections obtained by TEM. Channel dimensions are (width × depth) 1: 870 × 630 nm; 2: 240 × 410 nm; 3: 170 × 340 nm; 4: 150 × 180 nm. Width and depth measurements were taken at the centre line of the channels. Scale bar = 500 nm. (c) FIB milled channels aligned with the 100 μm wide reservoir channels in the PDMS cover slip. Scale bar = 1 mm. (d) Bright field TEM image showing the cross-section of a channel milled with similar conditions to channel 4. The FIB milling results in an amorphised silicon layer about 40 nm thick at the sample surface, visible as a slightly darker strip. The overlying black layer is metal deposited to protect the surface during sample preparation. Scale bar = 150 nm.

Data acquisition and processing

Experiments were carried out on a Zeiss LSM 510 confocal laser scanning microscope, using a 488 nm wavelength for excitation. The objective lenses used were a 40×/0.75 NA Plan-neofluar lens and a 63×/1.4 NA oil immersion Plan-neofluar lens.

Video sequences were recorded in real time at 25 frames per second (fps) using a CCD camera (LC365, Marconi Applied Technologies, UK) capable of video rate performance under low light conditions. Data output was analogue, in the form of interlaced frames at 25 fps. The monochromatic analogue output of the camera was digitised using a digital capture card (Coreco Imaging, Quebec, Canada), giving 8 bit greyscale images. Data was recorded direct to disk at 25 fps without data compression, using dedicated software (Video Savant v. 2.99, IO Industries, Ontario, Canada) which time-stamped each frame to the millisecond.

Sequences of interest were examined frame by frame and information on DNA position, visible dimensions and brightness obtained by image analysis. The interval between frames was 40 ms, but greater time resolution could be obtained by de-interlacing the raw data and examining it field-by-field. Video data was de-interlaced using Adobe Premiere v 5.1 (Adobe Systems Inc, USA) in order to improve the time resolution of the data.

Spatial calibration of the video data was carried out using a Richards microscope test slide (Structure Probe, Inc./SPI Supplies, West Chester, USA). Calibration gave image pixel sizes of 234 ± 2 nm horizontally and 233 ± 2 nm vertically. These data on distance and time allowed calculation of velocity of DNA moving under the influence of an applied voltage.

Results and discussion

Four channels were constructed as shown in Fig. 1a. Channel 1 is a straight-through channel with cross-sectional dimensions, 900 × 600 nm (width × depth). The remaining three channels varied in size from 250 × 400 nm (width × depth), down to 150 × 180 nm (Fig. 1b and c). These three channels were joined to connecting capillaries with dimensions 1000 × 1200 nm. The smallest nanocapillary was calculated to have a total volume of about 0.5 fl. Larger reservoir channels delivered the buffer–DNA solution to the four nanocapillaries (Fig. 1d). The overall arrangement of the electrophoretic device is given in Fig. 2.

The fabrication technique used here – gas-assisted direct FIB milling – is fast and flexible. However, the resulting channel cross-section tends to reflect the Gaussian density profile of the ion beam, as can be seen in Fig. 1b, particularly for the smallest channels which are of most interest in this study. While more information could be obtained by varying only depth or width while keeping the other channel dimensions constant, such control at the sub-100 nm scale is difficult using this direct milling technique. In future studies, a modified or alternative fabrication technique would be desirable.

In free solution and under the influence of an applied voltage, the dye-loaded λ-DNA molecules were observed to migrate in unmodified, coiled form through channel 1 and the connecting capillaries. However, on entering the nanocapillaries, DNA was observed to uncoil into a partially extended form. It appeared that once the DNA was inside the nanocapillaries, it experienced a very high degree of confinement, thereby affecting its dynamic behaviour.[11]

Both silicon, with a native oxide layer, and the formulation of PDMS[12] used in these experiments have an immobilized negative surface charge, and so support electro-osmotic flow towards the cathode. On the other hand, the DNA molecules, with an intrinsic negative charge, travel along the nanocapillaries one at a time towards the positive electrode. The observed movement of the

DNA towards the anode indicated that electrophoretic migration of the DNA dominated over any cathodic electro-osmotic flow of the buffer.

A molecule of λ-DNA, when naturally coiled in solution, has a radius of gyration $R_G \approx 800$ nm (calculated assuming a Flory coil and allowing for extension in the molecule length due to dye intercalation).[11,13] This is significantly larger than the cross-section of a nanocapillary and so the DNA will not enter unless driven by a process such as electrophoresis. At an applied voltage of 100 mV no DNA recruitment into the nanocapillaries was observed over several minutes. Above values of around 2 V, motion became too fast to allow satisfactory analysis. At intermediate voltages DNA migration could be recorded to show entry of DNA molecules at the cathodic end and exit at the anodic end of the nanocapillaries. On reversing polarity, DNA immediately reversed its direction of travel, and an individual molecule could be passed back and forth along a nanocapillary.

Fig. 3a shows stills taken from a video sequence. Many such sequences were observed for all the nanocapillaries. In this case the passage of a single DNA molecule through nanocapillary 2 (240 × 410 nm) is shown. In the first image (0 ms) a DNA molecule has just arrived at one end of the nanocapillary. The molecule is visible as a bright object approximately 1–1.5 μm in diameter, which is consistent with the calculated coil size. Before the DNA molecule can enter the opening there is an energy barrier to overcome. At lower applied voltages DNA frequently paused at the nanocapillary entrance, a phenomenon known as entropic trapping which has been exploited previously as a separation mechanism in planar slit structures with alternating thick and thin regions.[4,14] However, there is an important difference between planar slits and nanocapillaries. The trapping lifetime at the entrance to a slit depends on DNA size: a larger molecule has an increased interaction cross-section with the slit entrance. This is not the case at the entrance of a nanocapillary.[15] Provided the coil size is larger than the nanocapillary cross-section, the interaction cross-section and thus the trapping time will theoretically be independent of the molecular size.

In the second image (40 ms) part of the molecule has extended into the cathodic end of the nanocapillary. The next four images (80 ms to 180 ms) show the molecule inside the nanocapillary where it appears elongated. Frame by frame analysis of video sequences show visible DNA length within nanocapillaries to vary over a range of approximately 2 to 4 μm, with greater extensions the smallest structures. The molecule emerges at the anodic end, in this sequence at 200 ms, and immediately re-coils. On occasions where one or more further molecules entered a nanocapillary or the larger connecting capillary before the first molecule had exited, there was no noticeable effect on behaviour.

The brightness of coiled DNA molecules free in solution, as detected by the CCD camera both before and after translocation down the nanocapillary, was readily detectable. In comparison, the detected intensity of DNA molecules within the nanocapillaries was much fainter and appeared to reduce dramatically with smaller cross-sectional dimensions (see videoclip 1†). This effect seems larger than would be accounted for by coil extension alone. The reason for this is unclear but may be partly due to the smaller nanocapillaries having widths significantly less than both the excitation wavelength (491 nm in air) and the wavelength of the emitted light (509 nm). The video sequences† are key in providing additional insights into DNA behaviour within nanocapillaries and provide temporal information not available in the stills, including the rapid recovery of the original coiled form on exit.

Fig. 3b shows plots of velocity against position for DNA molecules traveling through the three smallest nanocapillaries;Fig. 3c shows similar plots for nanocapillary 3 at three different voltages applied across the device. Each plot is averaged from velocity *vs.* position results for seven individually tracked molecules. In each case the position was taken as the visible 'centre of mass' of the DNA, as the leading edge was often impossible to distinguish with any degree of certainty. As expected, the overall velocity increases with decreasing channel size and with higher applied voltages, both of which affect the magnitude of the electric field experienced by the DNA within the nanocapillaries. The plots show a generally consistent pattern of motion, with velocity tending to peak towards each end of the nanocapillary. The fluidic device was modeled using 2D finite element analysis software (Quickfield, v 4.2, Tera Analysis, California, USA) designed for electromagnetic, thermal and stress analysis. The right-hand graphs in Figs. 3b and 3c show the modeled results corresponding to the experimental results on the left, with the electric field values multiplied by a mobility value of 1×10^{-4} cm²/Vs. The peaks in the modeled results arise from distortion of the equipotential lines at the structure corners where the connecting channels abruptly neck down to the nanocapillaries. In the experimental results a similar double peak structure was frequently visible, as shown by the averaged results. The origin of the third velocity peak visible near the centre of nanocapillary 4 in Fig. 3b is currently unknown. At higher velocities the peaks appear to be displaced towards the centre of the nanocapillary section, and disappear entirely at the highest voltage shown for nanocapillary 3. The displacement of the peaks is thought to be an effect of the increased speed (resulting in fewer data points along a nanocapillary) and increased average extension associated with increased electric field strength.

For DNA undergoing free-solution electrophoresis we would expect a linear relationship $v = \mu E$, where v is the velocity, μ is the electophoretic mobility of the DNA and E is the electric field

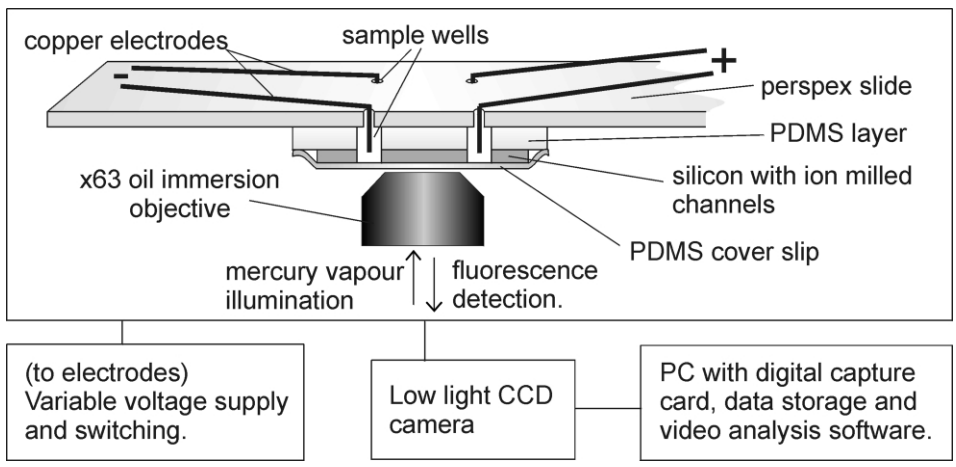

Fig. 2 Schematic diagram of the device, showing a cross-section through two of the sample wells. The intermediate PDMS layer forms a seal between the silicon and the slide. PDMS forms a tight reversible seal to a flat surface, allowing the structure to be disassembled and reused multiple times.

strength. Fig. 4a shows the variation of mean velocity with field strength for all four nanocapillaries. The dashed line is a reduced chi square linear regression through the origin, with a gradient corresponding to a mobility of $0.58 \pm 0.03 \times 10^{-4}$ cm^{2}V^{-1}s^{-1}. The data from the smallest nanocapillary lie consistently above the linear fit, and data from the largest lie consistently below the same line. This relationship is clearly illustrated in Fig. 4b which shows the variation in DNA mobility with nanocapillary size. From these data it is apparent that the mobility is greatest in the smallest nanocapillaries, *i.e.* for the same applied field the DNA travels fastest in the smallest channel, contrary to intuitive expectations.

The total mobility, μ, of the DNA within the structure is the vector sum of its electrophoretic mobility, μ_{ep}, and the electro-osmotic mobility of the buffer, μ_{eo} which in this case opposes μ_{ep}. The electrophoretic mobility is proportional to the DNA charge per unit length and inversely proportional to frictional drag. Even excluding interactions with the walls, hydrodynamic screening should increase the viscous drag as confinement increases.[11] In capillaries where the Debye length, characterizing the length scale of ionic interaction in solution, is no longer insignificant in comparison to the capillary half-width, the potential fields from opposite walls overlap.[16,17] As a result the velocity profile no longer attains the flat 'plug' flow characteristic of electro-osmotic flow (EOF) in larger channels but instead is parabolic with a reduced maximum fluid velocity. Wan[17] indicates that the EOF is reduced for $\kappa a < 20$, where κ is the reciprocal of the Debye length and a is the capillary radius. Burgreen and Nakache[18] predict that in the case of a tube or 'odd-shaped capillary' this reduction in flow becomes noticeable for an electrokinetic radius $\kappa a < 40$ (where a is the capillary half-width). For the conditions in this study we estimate a Debye length of 3.5 nm, resulting in electrokinetic radii of 34, 24 and 21 for nanocapillaries 2, 3 and 4 respectively. Therefore we interpret the observed increase in total mobility in the smallest nanocapillaries as a decrease in the opposing electro-osmotic mobility.

Nanocapillaries such as those demonstrated here, and knowledge of the extension behaviour and velocity of single molecules of DNA within nanocapillaries, could be applicable to emerging methods of DNA analysis. Single-molecule DNA mapping, using near-field optics and fluorescent markers to detect specific sequences, has been suggested.[5] However, to achieving higher spatial resolution in this technique there is a need for the detection device to contain a channel of the order of the persistence length of the DNA. This would force the molecule to enter the detection device not as a coil but as an extended strand. A practical realization of this requirement is strongly suggested by our results showing strand extension within nanocapillaries.

Another developing area of molecular analysis is concerned with the passage of molecules through nanopores. This approach has been assessed for sequencing single DNA molecules using ionic

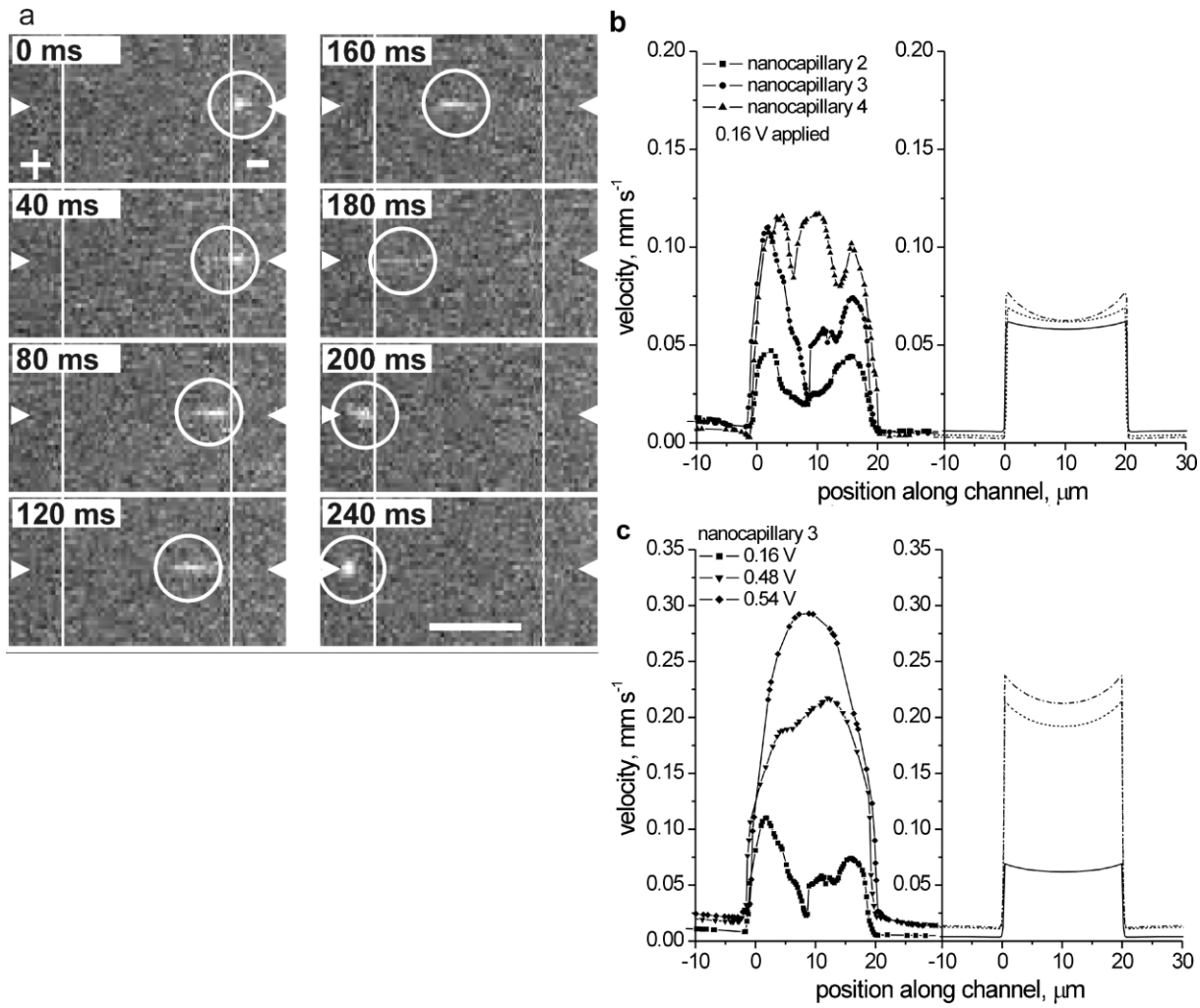

Fig. 3 Passage of single DNA molecules through a nanocapillary. (a) Sequence of deinterlaced video images showing the passage of a λ-DNA molecule (circled) through nanocapillary 2 (240 × 410 nm). The arrowheads on either side of each image mark the position of the connecting capillary and the vertical lines show the entrance and exit points for the nanocapillary. The voltage polarity is indicated at 0 ms and is the same for all the images. Scale bar = 10 μm. (b) Experimental (left) and modelled (right) results of DNA velocity *vs.* distance for individual molecules in nanocapillaries 2, 3 and 4 for the same voltage applied across the device. (c) Experimental (left) and modelled (right) results of DNA velocity *vs.* distance for individual molecules in nanocapillary 3 (170 × 340 nm) for different values of applied voltage. For the graphs, 0 μm corresponds to the entrance of the nanocapillary. All the experimental plots are the average of seven individually tracked molecules, and have a standard deviation of around 15% in each case.

conductance measurements across a natural nanopore (α-hemolysin ion channel) inserted into a lipid bilayer and exposed to an electric field.[6,7] This technique requires control of DNA velocity, so that the different current signatures of individual nucleotides can be more fully resolved as DNA molecules thread their way individually through the nanopore.[19] Schmidt *et al.*[20] have demonstrated electrophoretic self-positioning of charged lipid vesicles to form a lipid bilayer across a microfabricated aperture. Channel forming peptides subsequently introduced in solution self-assembled into the bilayer, allowing single ion channel conductance measurements. Next-generation nanocapillaries that would extend our present work may incorporate additional features, such as narrower cross-sections, constrictions, junctions and microfabricated, precisely positioned electrodes, to facilitate this objective by further physically constraining and controlling single DNA molecules *en route* to a nanopore. The approach of Schmidt *et al.*[20] could allow the use of natural nanopores in association with nanocapillaries as part of a larger fluidic device. Alternatively, man-made, molecular scale nanopores such as those fabricated in Si_3N_4[21] could be incorporated.

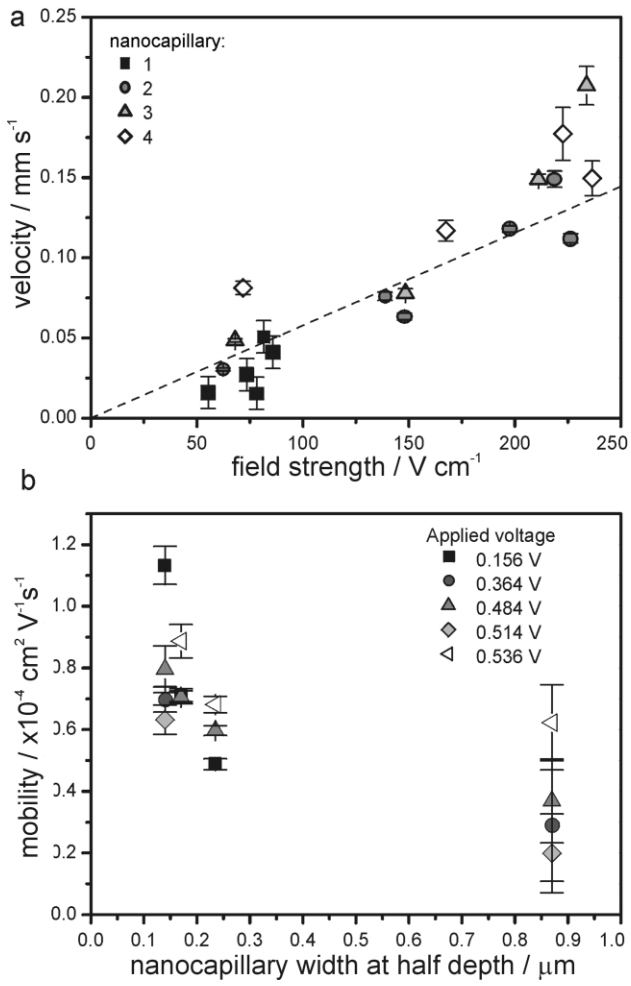

Fig. 4 Effect of nanocapillary size. (a) Velocity *vs.* field strength. The dashed line is a linear regression through the origin, the gradient corresponds to a mobility of $5.8 \pm 0.3 \times 10^{-5}$ $cm^2V^{-1}s^{-1}$. Experiments were carried out for several values of applied voltage. Each point is the mean of all measurements taken for one nanocapillary for each voltage. For capillaries 2–4 the errors shown are the standard error of the mean. The larger errors for data from nanocapillary 1 (900×600 nm) are due to flow from pressure differences across the device, which is insignificant for the smaller nanocapillaries. (b) Mobility *vs.* nanocapillary width. Mobility calculated as velocity divided by electric field strength, using the same data as Fig. 4a.

In conclusion, we have demonstrated the feasibility of incorporating nanocapillaries into a microfluidic structure and have shown active control of the velocity and direction of single molecules of DNA introduced into them. We believe such structures have great potential in biotechnology as an enabling device for single molecule manipulation, positioning and analysis.

Acknowledgements

We thank M. Fennah, H. Becker and I. Marshall for assistance and I. Moody and Marconi Applied Technologies for loan of the CCD camera. The work was funded by the EPSRC and GlaxoSmithKline.

References

1 A. Manz, N. Graber and H. M. Widmer, Miniaturized total chemical-analysis systems – a novel concept for chemical sensing, *Sens. Actuators, B*, 1990, **1**(1–6), 244–248.
2 M. Ueda, H. Nakanishi, O. Tabata and Y. Baba, Imaging of a band for DNA fragment migrating in microchannel on integrated microchip, *Mater. Sci. Eng., C*, 2000, **12**(1–2), 33–36.
3 W. D. Volkmuth and R. H. Austin, DNA electrophoresis in microlithographic arrays, *Nature*, 1992, **358**(6387), 600–602.
4 J. Han and H. G. Craighead, Separation of long DNA molecules in a microfabricated entropic trap array, *Science*, 2000, **288**(5468), 1026–1029.
5 C. F. Chou, R. H. Austin, O. Bakajin, J. O. Tegenfeldt, J. A. Castelino, S. S. Chan, E. C. Cox, H. Craighead, N. Darnton, T. Duke, J. Y. Han and S. Turner, Sorting biomolecules with microdevices, *Electrophoresis*, 2000, **21**(1), 81–90.
6 W. Vercoutere, S. Winters-Hilt, H. Olsen, D. Deamer, D. Haussler and M. Akeson, Rapid discrimination among individual DNA hairpin molecules at single-nucleotide resolution using an ion channel, *Nature Biotechnol.*, 2001, **19**, 248–252.
7 S. Howorka, S. Cheley and H. Bayley, Sequence-specific detection of individual DNA strands using engineered nanopores, *Nature Biotechnol.*, 2001, **19**, 636–639.
8 W. E. Booij, personal communication.
9 R. J. Young, J. R. A. Cleaver and H. Ahmed, Characteristics of gas-assisted focused ion-beam etching, *J. Vac. Sci. Technol. B*, 1993, **11**(2), 234–241.
10 L. R. Harriott, Focused-ion-beam-induced gas etching, *Jpn. J. Appl. Phys. Part 1 – Regul. Pap. Short Notes Rev. Pap.*, 1994, **33**(12B), 7094–7098.
11 O. B. Bakajin, T. A. J. Duke, C. F. Chou, S. S. Chan, R. H. Austin and E. C. Cox, Electrohydrodynamic stretching of DNA in confined environments, *Phys. Rev. Lett.*, 1998, **80**(12), 2737–2740.
12 G. Ocvirk, M. Munroe, T. Tang, R. Oleschuk, K. Westra and D. J. Harrison, Electrokinetic control of fluid flow in native poly(dimethylsiloxane) capillary electrophoresis devices, *Electrophoresis*, 2000, **21**, 107–115.
13 C. Carlsson, A. Larsson and M. Jonsson, Influence of optical probing with YOYO on the electrophoretic behavior of the DNA molecule, *Electrophoresis*, 1996, **17**(4), 642–651.
14 J. Han, S. W. Turner and H. G. Craighead, Entropic trapping and escape of long DNA molecules at submicron size constriction, *Phys. Rev. Lett.*, 1999, **83**(8), 1688–1691.
15 S. Daoudi and F. Brochard, Flows of flexible polymer solutions in pores, *Macromolecules*, 1978, **11**(4), 751–758.
16 C. L. Rice and R. Whitehead, Electrokinetic Flow in a Narrow Cylindrical Capillary, *J. Phys. Chem.*, 1965, **69**(11), 4017–4024.
17 Q. H. Wan, Effect of electrical double-layer overlap on the electro-osmotic flow in packed-capillary columns, *Anal. Chem.*, 1997, **69**(3), 361–363.
18 D. Burgreen and F. R. Nakache, Electrokinetic flow in ultrafine capillary slits, *J. Phys. Chem.*, 1964, **68**(5), 1084–1091.
19 H. Wang and D. Branton, Nanopores with a spark for single-molecule detection, *Nature Biotechnol.*, 2001, **19**, 622–623.
20 C. Schmidt, M. Mayer and H. Vogel, A Chip-Based Biosensor for the Functional Analysis of Single Ion Channels, *Angew. Chem. Int. Ed.*, 2000, **39**(17), 3137–3140.
21 L. Jiali, D. Stein, C. McMullan, D. Branton, M. J. Aziz and J. A. Golovchenko, Ion-beam sculpting at nanometre length scales, *Nature*, 2001, **412**, 166–169.